

AperTO - Archivio Istituzionale Open Access dell'Università di Torino

Photoinduced transformation of pyridinium-based ionic liquids, and implications for their photochemical behavior in surface waters

This is the author's manuscript

Original Citation:

Availability:

This version is available <http://hdl.handle.net/2318/1647316> since 2017-09-07T15:10:21Z

Published version:

DOI:10.1016/j.watres.2017.05.064

Terms of use:

Open Access

Anyone can freely access the full text of works made available as "Open Access". Works made available under a Creative Commons license can be used according to the terms and conditions of said license. Use of all other works requires consent of the right holder (author or publisher) if not exempted from copyright protection by the applicable law.

(Article begins on next page)

This Accepted Author Manuscript (AAM) is copyrighted and published by Elsevier. It is posted here by agreement between Elsevier and the University of Turin. Changes resulting from the publishing process - such as editing, corrections, structural formatting, and other quality control mechanisms - may not be reflected in this version of the text. The definitive version of the text was subsequently published in WATER RESEARCH, 122, 2017, 10.1016/j.watres.2017.05.064.

You may download, copy and otherwise use the AAM for non-commercial purposes provided that your license is limited by the following restrictions:

- (1) You may use this AAM for non-commercial purposes only under the terms of the CC-BY-NC-ND license.
- (2) The integrity of the work and identification of the author, copyright owner, and publisher must be preserved in any copy.
- (3) You must attribute this AAM in the following format: Creative Commons BY-NC-ND license (<http://creativecommons.org/licenses/by-nc-nd/4.0/deed.en>), 10.1016/j.watres.2017.05.064

The publisher's version is available at:

<http://linkinghub.elsevier.com/retrieve/pii/S0043135417304281>

When citing, please refer to the published version.

Link to this full text:

<http://hdl.handle.net/2318/1647316>

Photoinduced transformation of pyridinium-based ionic liquids, and implications for their photochemical behavior in surface waters

Paola Calza⁽¹⁾, Giorgio Noè⁽¹⁾, Debora Fabbri⁽¹⁾, Valentina Santoro⁽²⁾, Claudio Minero⁽¹⁾,
Davide Vione*⁽¹⁾, Claudio Medana⁽²⁾

(1) Department of Chemistry, University of Torino, via P. Giuria 5, 10125 Torino, Italy

*(2) Department of Molecular Biotechnology and Health Sciences, University of Torino, via P. Giuria 5, 10125
Torino, Italy*

* Corresponding author. E-mail: davide.vione@unito.it

Abstract

The photochemical reactivity of three ionic liquids (1-ethylpyridinium tetrafluoroborate, 1-butyl-4-methylpyridinium tetrafluoroborate, and 1-(3-cyanopropyl)pyridinium chloride) was studied by combining laboratory experiments and photochemical modeling, to get insight into the possible behavior in surface-water environments. Among the studied compounds, phototransformation in sunlit surface waters could be an important attenuation pathway for 1-butyl-4-methylpyridinium tetrafluoroborate (BMPOTFB). In this case the reaction with the carbonate radicals ($\text{CO}_3^{\cdot-}$) would prevail at low values of the dissolved organic carbon (DOC), while the direct photolysis would be important at intermediate to high DOC values. The sensitization by the triplet states of chromophoric dissolved organic matter could play a significant role at high DOC, especially in the presence of a considerable fraction of highly photoreactive pedogenic organic matter derived from soil runoff. The main processes that account for the phototransformation of BMPOTFB and produce the main detected transformation products (TPs) are hydroxylation, detachment/shortening of the butyl chain and double bond formation. Interestingly, there is a considerable overlap between the intermediates formed by direct photolysis and those produced by indirect photochemistry. Some of the TPs formed from BMPOTFB are more toxic than the parent compound towards *Vibrio fischeri* bacteria, and account for the increase in toxicity of the irradiated mixtures. Differently from BMPOTFB, in the case of the other two studied ionic liquids the photodegradation would play a negligible role in environmental attenuation, with the possible exception of very shallow waters with low DOC.

Keywords: pollutants in surface waters; environmental attenuation of pollution; sunlight-induced reactions; direct and indirect photochemistry.

31 **1. Introduction**

32 Ionic liquids (ILs) have several interesting properties such as good thermal stability, wide
33 electrochemical potential window, high electric conductivity and miscibility with water or organic
34 solvents, which permit application mainly as solvents for organic synthesis and as electrolytes
35 (Plechko and Seddon, 2008; Holbrey and Seddon, 1999). Room-temperature ILs have received
36 huge attention as green and high-tech reaction media (Stepnowski and Zaleska, 2005) because,
37 differently from conventional organic solvents, they have negligible vapor pressure and do not emit
38 toxic vapors (Kralisch et al 2005).

39 However, a broad implementation of the use of ILs in industry may have some drawbacks. For
40 instance, due to their high stability, significant amounts of ILs are expected to occur in natural
41 waters and soil in the near future (Bubalo et al. 2014; Czerwicka et al. 2009; Richardson and
42 Ternes, 2014). Surface water is a major environmental compartment in which ILs may be emitted as
43 industrial wastes, and the most hydrophilic of these compounds should preferentially be found in
44 aqueous phases. Therefore, information concerning the fate of ILs in the aquatic environment is
45 crucial. Some studies have shown that ILs are more toxic to cells than conventional solvents
46 (Stepnowski and Zaleska, 2005), and the most common imidazolium-based compounds also
47 showed high resistance against microbial degradation (Czerwicka et al, 2009).

48 Photochemistry is a potentially important attenuation route for ILs in surface waters (Calza et al.,
49 2015). Generally speaking, phototransformation in surface waters can be divided into direct
50 photolysis (a xenobiotic absorbs sunlight, which triggers its degradation) and indirect
51 photochemistry. In the latter, sunlight is absorbed by naturally-occurring photosensitizers (most
52 notably nitrate, nitrite and chromophoric dissolved organic matter, CDOM) to produce reactive
53 transient species ($\bullet\text{OH}$, $^1\text{O}_2$ and CDOM triplet states, $^3\text{CDOM}^*$) (Dong et al., 2015; Rosario-Ortiz
54 and Canonica, 2016). More precisely, nitrate and nitrite yield $\bullet\text{OH}$, while irradiated CDOM
55 produces $^3\text{CDOM}^*$, which can form $^1\text{O}_2$ by reaction with oxygen (McNeill and Canonica, 2016).

Irradiated CDOM yields $\bullet\text{OH}$ as well (Lee et al., 2013; Page et al., 2014), at least partially through a photo-Fenton process (Chiwa et al., 2015; Mostofa and Sakugawa, 2016; Giannakis et al., 2016a/b). An additional transient, the carbonate radical $\text{CO}_3^{\bullet-}$, is produced by oxidation of carbonate and bicarbonate by $\bullet\text{OH}$ and of carbonate by $^3\text{CDOM}^*$ (Canonica et al., 2005; Bahnmuller et al., 2014; Janssen et al., 2014; Trivella et al., 2015; Bintou et al., 2015). These transients are then involved into the phototransformation of xenobiotics (Silva et al., 2015), including the xenobiotics that do not undergo direct photolysis (Janssen et al., 2015). Dissolved organic matter (DOM, not necessarily chromophoric), which is usually quantified as the dissolved organic carbon (DOC), is the main sink of both $\bullet\text{OH}$ and $\text{CO}_3^{\bullet-}$ (Huang and Mabury, 2000; Canonica et al., 2005; Keen et al., 2014). This issue, combined with the fact that CDOM is a major radiation absorber, explains why $\bullet\text{OH}$ and $\text{CO}_3^{\bullet-}$ are usually more concentrated in low-DOC waters. In contrast, the highest levels of $^3\text{CDOM}^*$ and $^1\text{O}_2$ usually occur in high-DOC environments, because organic matter is involved in the production of these transients but not in their scavenging. Actually, the quenching of $^3\text{CDOM}^*$ occurs by reaction with O_2 or internal conversion, while $^1\text{O}_2$ is quenched by collision with the water solvent (Wenk et al., 2013; Vione et al., 2014).

Within this framework, we studied the photofate of three pyridinium-based ILs under conditions that are relevant to sunlit environmental waters: 1-ethylpyridinium tetrafluoroborate (EPTFB), 1-(3-cyanopropyl)pyridinium chloride (CPPC) and 1-butyl-4-methylpyridinium tetrafluoroborate (BMPOTFB). The known physical properties of the studied ILs (Zhao et al., 2003; Bandres et al., 2008; Guerrero et al., 2012) are summarized in **Table SM1** in the Supplementary Material (hereafter SM). We paid attention to the identification of the intermediate products formed during ILs degradation, by using the HPLC-MS/MS technique. The identification of transformation products (TPs) is a crucial aspect because, in addition to providing important information on the mechanism of degradation, the formed TPs may have a very different impact on the environment

compared to the parent molecules. To our knowledge, this is the first study about the photochemical transformation of EPTFB, CPPC and BMPOTFB.

2. Experimental section

2.1. Materials and Reagents

1-Ethylpyridinium tetrafluoroborate (**EPTFB**) (98%), 1-(3-cyanopropyl)pyridinium chloride (**CPPC**) (98.5%), 1-butyl-4-methylpyridinium tetrafluoroborate (**BMPOTFB**) ($\geq 97,0\%$), sodium nitrate ($\geq 99,9\%$), sodium bicarbonate ($\geq 99,7\%$), acetonitrile ($\geq 99\%$), acetaminophen (APAP), anthraquinone-2-sulfonic acid, sodium salt (98%), hydrogen peroxide (35%), formic acid (98%), sodium 1-hexanesulfonate (98%), and phosphoric acid (85%) were purchased from Sigma Aldrich, Italy. Rose Bengal (80%) was purchased from Alfa Aesar. All aqueous solutions were prepared with ultra-pure water (Millipore Milli-QTM).

2.2. Irradiation Experiments

Irradiation experiments were performed in magnetically stirred cylindrical closed cells (Pyrex glass, 40 mm i.d. \times 25 mm), on 5 mL aqueous solutions containing each studied IL at 20 μ M initial concentration. The goal of these experiments was not to directly reproduce environmental conditions in the laboratory (which is indeed problematic, in particular as far as the water depth is concerned), but rather to obtain reasonably accurate measurements of the main photochemical parameters such as direct photolysis quantum yields and second-order reaction rate constants. These data, used as input values for a photochemical model, allow inferences to be made on the photochemical fate of the studied compounds in environmental waters. Direct photolysis experiments were carried out on each IL taken separately, under UVB irradiation with a Philips TL 20W/01 RS lamp having emission maximum at 313 nm. The lamp radiation reached the irradiated solutions mainly from the top.

Indirect photolysis experiments followed the competition kinetics approach (Puskas et al., 2005; Dantas et al., 2007; Katsoyiannis et al., 2011; Sun et al., 2016). They were run on systems containing a mixture of all the studied ILs and acetaminophen (APAP), each at 20 μ M initial concentration. The rationale for the use of APAP as reference compound is that its second-order reaction rate constants are known for all the transient species relevant to this study (\bullet OH, $\text{CO}_3^{\bullet-}$, $^1\text{O}_2$ and $^3\text{CDOM}^*$; De Laurentiis et al., 2014). An important issue in these competition kinetics experiments is the need to minimize the occurrence of multiple reaction pathways, which are problematic for the assessment of the reaction rate constants. For the competition approach to work, one needs a single prevailing reaction pathway to be operational. Therefore, the radical \bullet OH was produced by irradiating 100 mM NaNO_3 under the TL 01 RS lamp described above, which was also used to produce $\text{CO}_3^{\bullet-}$ upon irradiation of 100 mM NaNO_3 + 100 mM NaHCO_3 . In both cases, a high concentration of nitrate was used to minimize the IL direct photolysis. Elevated bicarbonate was needed to scavenge the majority of photogenerated \bullet OH, thereby minimizing the interference of \bullet OH on the $\text{CO}_3^{\bullet-}$ reactions. Anthraquinone-2-sulfonate (AQ2S) was used as CDOM proxy to study the reactivity of $^3\text{CDOM}^*$. The use of AQ2S has pros and cons: on the one side it does not yield \bullet OH or $^1\text{O}_2$ upon irradiation, which allows for the study of a pure triplet-sensitized process (Maddigapu et al., 2010). In the case of atrazine, a remarkably good agreement has also been found between the reaction rate constants with $^3\text{AQ2S}^*$ and with natural $^3\text{CDOM}^*$ (Marchetti et al, 2013; Zeng and Arnold, 2013). However, the triplet state $^3\text{AQ2S}^*$ may be more reactive than average $^3\text{CDOM}^*$, which could lead to an overestimation of the triplet-sensitization rate constants when using AQ2S as CDOM proxy (De Laurentiis et al., 2014; Avetta et al., 2016). The latter issue should be (and was here) taken into account when using kinetic data derived from AQ2S photochemistry. In the AQ2S experiments, solutions containing 0.2 mM AQ2S and 20 μ M ILs/APAP mixtures were irradiated under a Philips TLK 05 lamp, with emission maximum at 365 nm. Finally, measures of reactivity with $^1\text{O}_2$ were performed using a lamp Philips TL D 18W/16

with emission maximum at 545 nm. The dye Rose Bengal (10 μ M initial concentration) was chosen as the $^1\text{O}_2$ source. The irradiation conditions already described were also used for the study of IL transformation products (TPs) *via* the aforementioned photochemical pathways. In this case, however, each IL was irradiated separately and at a relatively high loading (20 mg L⁻¹), to simplify TPs detection and identification.

2.3. Analytical Procedures

2.3.1. Liquid Chromatography - UV detection (HPLC-UV)

After the scheduled irradiation times the cells were withdrawn from the lamp, and their content was analyzed by HPLC-UV to monitor the time evolution of the studied ILs and, when relevant, of APAP as well. The instrument used was a Merck-Hitachi HPLC equipped with AS-2000A autosampler (100 μ L injection volume), L-6200 and L-6200A pumps for high-pressure gradients, L-4200 UV-Vis detector and a reverse-phase column Phenomenex Kinetex® 100Å C18 (250 mm \times 4.6 mm \times 5 μ m). The eluent consisted of an aqueous solution of the ionic coupler sodium 1-hexanesulfonate 0.01 M (eluent A) and acetonitrile (eluent B). After 3 min of isocratic conditions (90/10 v/v A/B), the acetonitrile fraction was increased up to 60/40 v/v in 19 min. For the tests with the dye Rose Bengal these conditions were followed by a second gradient up to 40/60 v/v A/B over 4 min, which was held for 5 min to allow elution of the photosensitizer. Re-equilibration of the HPLC column was achieved by going back to the starting conditions, which were held for 5 min before the next injection. The mobile phase flow rate was 1 mL/min and the detection wavelength was 210 nm. With these elution conditions the retention times were 5.3 min for APAP, 6.2 min for EPTFB, 6.8 min for CPPC, and 14.6 min for BMPOTFB.

2.3.2. Liquid Chromatography - High Resolution Mass Spectrometry (HPLC-HRMS)

This technique was used to detect and identify the TPs of the studied ILs under irradiation. For HPLC-HRMS analyses of the irradiated aqueous solutions, the chromatographic separations were carried out with a Phenomenex C18 Gemini® NX 110-Å column, 150 mm \times 2.1 mm \times 3 μ m

154 particle size (Phenomenex, Bologna, Italy), using a Ultimate 3000 HPLC instrument (Dionex,
155 Thermo Scientific, Milan, Italy). The injection volume was 20 μ L and the flow rate 200 μ L/min. A
156 gradient mobile phase composition was used, going from 5/95 v/v of acetonitrile/
157 heptafluorobutyric acid (5 mM in water) to 20/80 v/v in 15 min, followed by a second gradient step
158 up to 95/5 v/v in 5 min.

159 A LTQ Orbitrap mass spectrometer (Thermo Scientific, Milan, Italy) was interfaced to the HPLC
160 instrument through an ESI ion source. The HPLC column effluent was delivered into the ion source
161 using nitrogen as both sheath and auxiliary gas. The capillary voltage and tube lens voltage in the
162 ESI source were maintained at 28 V and 70 V, respectively. The source voltage was set to 4.5 kV in
163 the positive ion mode. The capillary temperature was maintained at 270°C. The acquisition method
164 was optimized beforehand in the tuning sections (capillary, magnetic lenses and collimating
165 octapole voltages) for the parent compound, to achieve maximum sensitivity. Mass accuracy of the
166 recorded ions (vs calculated) was \pm 5 millimass units (mmu, without internal calibration).

167 The MS spectra were acquired using full scan MS (50-1000 m/z range) and MS² acquisition in the
168 positive ion mode, with a resolution of 30000 (500 m/z FWHM) in FTMS (full transmission) mode.
169 The ions submitted to MS² acquisition were chosen on the basis of full MS spectra abundance,
170 without using automatic dependent scan. Collision energy was set to 30% for all of the MS²
171 acquisition methods, and the MS² acquisition range was between the value of ion trap cut-off and
172 the m/z value of the (M+H)⁺ ion. Xcalibur software (Thermo Scientific, Milan, Italy) was used for
173 both acquisition and data analysis.

174 2.3.3. Toxicity Measurements

175 The toxicity of the reaction mixtures collected at different irradiation times was measured with a
176 Microtox® Model 500 Toxicity Analyzer (Milan, Italy). Acute toxicity was assessed with a
177 bioluminescence inhibition assay using the marine bacterium *Vibrio fischeri*, by monitoring changes
178 in the natural emission of the luminescent bacteria when challenged with toxic compounds. Freeze-

179 dried bacteria, reconstitution solution, diluent (2% NaCl) and an adjustment solution (non-toxic
 180 22% sodium chloride) were purchased from Azur (Milan, Italy). Samples were tested in five
 181 dilutions in a medium containing 2% sodium chloride, and luminescence was recorded after 5, 15,
 182 and 30 min of incubation at 15°C. Because no substantial changes in luminescence were observed
 183 between 5 and 30 minutes, only the percent toxicity recorded at 15 minutes will be discussed.
 184 Inhibition of luminescence, compared with a toxic-free control to give the percentage inhibition,
 185 was calculated following the established protocol of the Microtox® calculation program.

186 **2.4. Kinetic data treatment**

187 The time evolution of the studied ILs was fitted with a pseudo-first order equation of the form
 188 $C_t^{IL} = C_o^{IL} e^{-k_{IL} t}$, where C_t^{IL} is the IL concentration at the time t , C_o^{IL} the initial concentration, and k_{IL}
 189 the pseudo-first order degradation rate constant. The IL initial degradation rate was calculated as
 190 $R_o^{IL} = k_{IL} C_o^{IL}$. The initial degradation rate of APAP (R_o^{APAP}) was calculated in a similar way.

191 With a mixture of APAP and of the studied ILs, under conditions where a reactive species X is
 192 generated (with $X = \bullet OH, CO_3^{\bullet-}, ^1O_2$ or $^3AQ2S^*$), if reaction with X only is operational, the initial
 193 rate is $R_o^{IL} = k_{X,IL}[X]C_o^{IL}$ for each relevant IL, and $R_o^{APAP} = k_{X,APAP}[X]C_o^{APAP}$ for APAP. Here, $k_{X,IL}$
 194 and $k_{X,APAP}$ are the respective second-order reaction rate constants of X with each studied IL and
 195 with APAP, and $[X]$ is the steady-state concentration of the transient species. Because ILs and
 196 APAP occur together in the same mixture, $[X]$ is the same in all the relevant expressions of R_o^{IL} and
 197 R_o^{APAP} . Moreover, we chose the initial conditions so that $C_o^{IL} = C_o^{APAP}$. On this basis it is possible to
 198 derive $R_o^{IL}(R_o^{APAP})^{-1} = k_{X,IL}(k_{X,APAP})^{-1}$, from which the second-order rate constant of the reaction
 199 between each IL and X can be obtained as follows: $k_{X,IL} = k_{X,APAP} R_o^{IL}(R_o^{APAP})^{-1}$ (Herrmann et al.,
 200 2010). Note that the initial rates are derived from the experimental data, while $k_{X,APAP}$ is known
 201 from a previous study (De Laurentiis et al., 2014).

For the determination of the direct photolysis quantum yields, the photon flux absorbed by each IL (P_a^{IL}) was calculated as follows: $P_a^{IL} = \int_{\lambda} p^{\circ}(\lambda)[1 - 10^{-\varepsilon_{IL}(\lambda)b[IL]}]d\lambda$, where $p^{\circ}(\lambda)$ is the incident spectral photon flux density of the used UVB lamp, $\varepsilon_{IL}(\lambda)$ is the IL molar absorption coefficient, $b = 0.4$ cm is the optical path length inside the solution, and $[IL] = 20\mu\text{L}$ is the initial molar concentration of the relevant IL. The values of $p^{\circ}(\lambda)$ were determined by combining spectral measurements with a calibrated Ocean Optics USB2000 CCD spectrophotometer, and chemical actinometry with 2-nitrobenzaldehyde. The detailed procedure has been reported by Marchisio et al. (2015). The wavelength trends of $p^{\circ}(\lambda)$ and $\varepsilon_{IL}(\lambda)$ are shown in **Figure 1A**. The direct photolysis quantum yield was calculated as $\Phi_{IL} = R_o^{IL}(P_a^{IL})^{-1}$.

2.5. Photochemical modeling

The model assessment of ILs photodegradation was carried out with the APEX software (Aqueous Photochemistry of Environmentally-occurring Xenobiotics), available for free as Electronic Supplementary Information of Bodrato and Vione (2014). APEX predicts photochemical reaction kinetics from photoreactivity parameters of xenobiotics (absorption spectra, direct photolysis quantum yields and second-order reaction rate constants with transient species), and from data of water chemistry and depth (Bodrato and Vione, 2014). APEX predictions have been validated by comparison with field data of pollutant phototransformation kinetics in surface freshwaters (Marchetti et al., 2013; Avetta et al., 2016). The standard solar spectrum used in APEX is referred to fair-weather conditions during summertime at mid latitude (Frank and Klöpffer, 1988). Sunlight irradiance is not constant in the natural environment, due to fluctuations in meteorological conditions (not included in APEX) and to diurnal and seasonal cycles. To allow easier comparison between model results and environmental conditions, taking the day-night cycle into account, APEX uses a summer sunny day (SSD) as time unit, equivalent to fair-weather 15 July at 45° N latitude. The absorption of radiation by the photosensitisers (CDOM, nitrate and nitrite) and the

226 studied substrates is calculated based on competition for sunlight irradiance in a Lambert-Beer
227 approach (Bodrato and Vione, 2014; Braslavsky, 2007). APEX applies to well-mixed waters and
228 gives average values over the water column, with contributions from the well-illuminated surface
229 layer and from darker water in the lower depths, where irradiance is very low (Loiselle et al., 2008).

230

231 **3. Results and Discussion**

232 **3.1. Photochemical reactivity of the studied ILs**

233 First of all, the direct photolysis of **EPTFB**, **CPPC** and **BMPOTFB** was studied by irradiating the
234 relevant compounds taken separately (no mixtures were used in this case) under a UVB lamp. The
235 ILs time trends are reported in **Figure 1B**, which shows that the photochemical degradation rates
236 followed the order **BMPOTFB** > **CPPC** > **EPTFB**. The relevant direct photolysis quantum yields
237 are reported in **Table 1**. The comparison between quantum yield values (**Table 1**) and
238 photodegradation kinetics (**Figure 1B**) suggests that **EPTFB** was the compound featuring both the
239 lowest quantum yield of direct photolysis (about one order of magnitude smaller than the other two
240 ILs) and the slowest direct phototransformation. Compared with the other studied ILs, **EPTFB**
241 featured an intermediate degree of UVB radiation absorption (**Figure 1A**). **CPPC** was the studied
242 IL with the highest quantum yield of direct photolysis but, because of relatively low radiation
243 absorption, its photodegradation was slower compared to **BMPOTFB**.

244 The reactivity between the studied ILs and the transient species under consideration ($X = \bullet\text{OH}$,
245 $\text{CO}_3^{\bullet-}$, $^1\text{O}_2$ or $^3\text{AQ2S}^*$) was studied in mixtures of **EPTFB**, **CPPC**, **BMPOTFB** and APAP
246 (hereafter, substrates). All of the four substrates had the same initial concentration in the mixture
247 ($[\text{Substrate}]_0 = 20 \mu\text{M}$). The reaction with $\bullet\text{OH}$ was studied upon UVB irradiation of the mixture in
248 the presence of 0.10 M NaNO_3 , and the reactivity order was **BMPOTFB** > **EPTFB** > **CPPC**. The
249 substrates time evolution is shown in **Figure 2A**, while the second-order reaction rate constants of
250 the studied ILs with $\bullet\text{OH}$ are listed in **Table 1**.

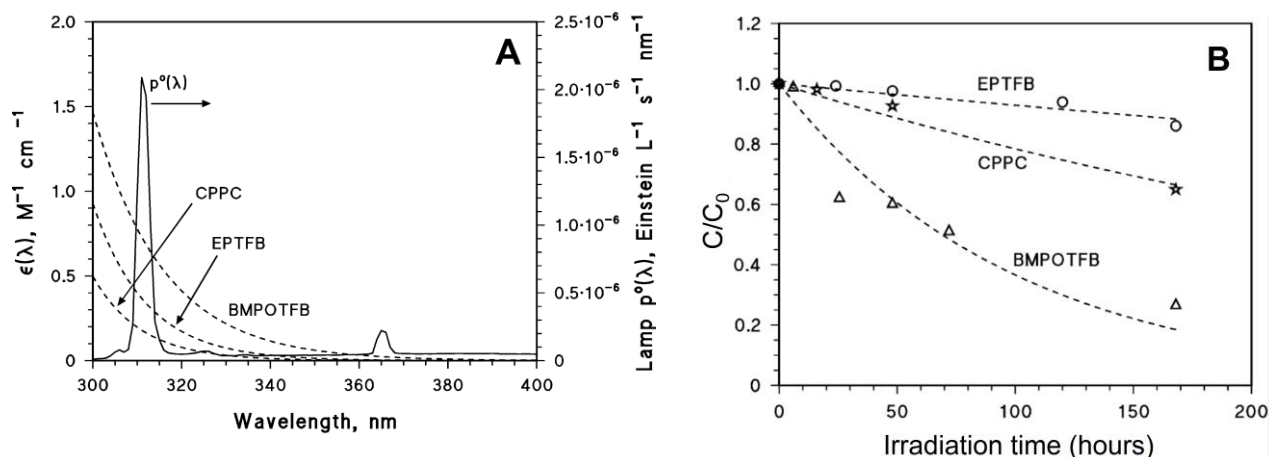
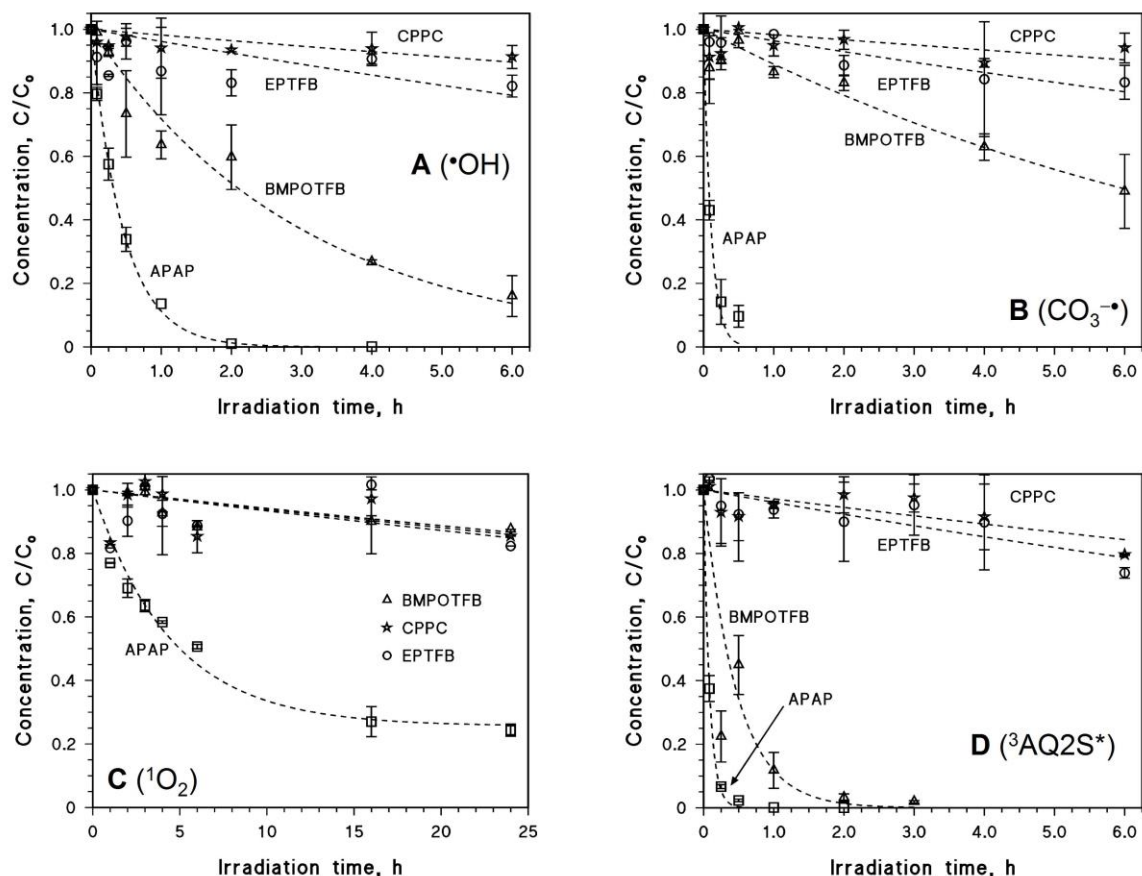


Figure 1. (A) Absorption spectra ($\epsilon(\lambda)$) of the studied ILs, and emission spectrum ($p^\circ(\lambda)$) of the used UVB lamp (Philips TL 01). (B) Time trends of the studied ILs (each had a 20 μ M initial concentration in a distinct one-component solution) upon UVB irradiation in Milli-Q water (direct photolysis experiments).

Table 1. Photoreactivity parameters (direct photolysis quantum yields and second-order reaction rate constants with photoinduced transients) of the studied ILs and of APAP. For modeling purposes, the range of $k_{IL,^3CDOM^*}$ was varied between $0.05 k_{IL,^3AQ2S^*}$ and $k_{IL,^3AQ2S^*}$ as explained in the text. Note that Substrate = EPTFB, BMPOTFB, CPPC, or APAP. The APAP data are taken from De Laurentiis et al. (2014). Φ_{APAP} is reported for a sake of completeness, but it was not used to calculate Φ_{IL} . The error bounds, representing the σ -level uncertainty, were taken from the literature in the case of APAP. For the studied ILs, they were derived from duplicate experiments.

	EPTFB	BMPOTFB	CPPC	APAP
$\Phi_{Substrate}$, unitless	$(4.81 \pm 0.62) \cdot 10^{-2}$	$(4.53 \pm 0.62) \cdot 10^{-1}$	$(7.77 \pm 0.67) \cdot 10^{-1}$	$(4.57 \pm 0.17) \cdot 10^{-2}$
$k_{Substrate^{\bullet}OH}$, $M^{-1} s^{-1}$	$(3.33 \pm 2.23) \cdot 10^7$	$(2.84 \pm 1.22) \cdot 10^8$	$(1.55 \pm 0.91) \cdot 10^7$	$(1.87 \pm 0.56) \cdot 10^9$
$k_{Substrate^{\bullet}CO_3^-}$, $M^{-1} s^{-1}$	$(7.04 \pm 5.97) \cdot 10^5$	$(4.85 \pm 2.59) \cdot 10^6$	$(1.52 \pm 0.86) \cdot 10^6$	$(3.8 \pm 1.1) \cdot 10^8$
$k_{Substrate^{\bullet}O_2}$, $M^{-1} s^{-1}$	$(1.40 \pm 1.30) \cdot 10^6$	$(1.50 \pm 1.10) \cdot 10^6$	$(1.30 \pm 1.10) \cdot 10^6$	$(3.68 \pm 0.73) \cdot 10^7$
$k_{Substrate^{\bullet}AQ2S^*}$, $M^{-1} s^{-1}$	$(3.71 \pm 1.17) \cdot 10^7$	$(1.99 \pm 1.18) \cdot 10^9$	$(2.64 \pm 0.99) \cdot 10^7$	$(1.08 \pm 0.16) \cdot 10^{10}$



265

266 **Figure 2.** Time trends of APAP and the three studied ILs in the same mixture (20 μM initial
 267 concentration for each substrate), in the presence of: (A) 0.1 M NaNO_3 under UVB irradiation; (B)
 268 0.1 M NaNO_3 + 0.1 M NaHCO_3 under UVB irradiation; (C) 10 μM Rose Bengal under yellow-
 269 lamp irradiation; (D) 0.2 mM AQ2S under UVA irradiation. The error bars represent the standard
 270 error of duplicate experiments.

271

272

273 The reaction with $\text{CO}_3^{\bullet-}$ was studied upon UVB irradiation of 0.1 M NaNO_3 + 0.1 M NaHCO_3 ,
 274 under which conditions the $\bullet\text{OH}$ radicals generated by nitrate photolysis would be largely (>95%)
 275 scavenged by the HCO_3^- and CO_3^{2-} ions to produce $\text{CO}_3^{\bullet-}$. The $\bullet\text{OH}$ scavenging fractions were
 276 assessed on the basis of the known $\bullet\text{OH}$ reaction rate constants of HCO_3^- and CO_3^{2-} (Buxton et al.,
 277 1988), of the rate constants of the studied substrates (**Table 1**), and on the initial concentrations in

278 solution. The ILs order of reactivity with $\text{CO}_3^{\bullet-}$ was **BMPOTFB** > **EPTFB** > **CPPC**. The relevant
279 time evolutions are shown in **Figure 2B**, and the second-order reaction rate constants are listed in
280 **Table 1**.

281 The transient $^1\text{O}_2$ was generated by irradiation of 10 μM Rose Bengal under yellow light. The three
282 ILs showed comparably low reactivity with $^1\text{O}_2$, much lower than for APAP (see **Figure 2C** and
283 **Table 1**). Finally, the reactivity by triplet sensitization was studied upon UVA irradiation of 0.2
284 mM AQ2S, a concentration value that was chosen to minimize the reaction between excited and
285 ground-state AQ2S (Bedini et al., 2012). Also in this case the reactivity order was **BMPOTFB** >
286 **EPTFB** > **CPPC** (see **Figure 2D** and **Table 1**).

287 As explained before, $^3\text{AQ2S}^*$ may be more reactive than natural $^3\text{CDOM}^*$ and may provide an
288 overestimation of the $^3\text{CDOM}^*$ rate constants (De Laurentiis et al., 2014; Avetta et al., 2016). For
289 this reason, and based on the results of a recent study (Avetta et al., 2016), the $^3\text{AQ2S}^*$ rate
290 constants ($k_{IL,^3\text{AQ2S}^*}$) were taken as upper limits for those with $^3\text{CDOM}^*$ ($k_{IL,^3\text{CDOM}^*}$). The
291 corresponding lower limits were taken as $k_{IL,^3\text{CDOM}^*} = 0.05 k_{IL,^3\text{AQ2S}^*}$. By assuming that $k_{IL,^3\text{CDOM}^*}$
292 varies between $0.05 k_{IL,^3\text{AQ2S}^*}$ and $k_{IL,^3\text{AQ2S}^*}$, one gets some insight into the potentially variable
293 reactivity of $^3\text{CDOM}^*$. Indeed, triplet sensitisation processes are quite fast when triggered by
294 runoff-derived soil organic matter, and they are much slower in the presence of aquagenic CDOM
295 (De Laurentiis et al., 2012).

296 In the above experiments of indirect photochemistry it was generally found that **BMPOTFB** had a
297 significantly higher reactivity than the other studied ILs, but it was less reactive than APAP. All
298 three ILs have an electron-poor pyridinium ring, which might account for lower reactivity with
299 oxidizing transient species when compared to the electron-rich phenolic ring of APAP. However,
300 differently from the other ILs, **BMPOTFB** also has an electron-donating methyl substituent that

could somewhat increase the electron density on the aromatic ring and, therefore, make it more reactive than the other studied ILs.

3.2. Modeling of ILs phototransformation in surface waters

The photoreactivity parameters reported in **Table 1** were used as input data for the APEX software, using either $k_{IL,^3CDOM^*} = k_{IL,^3AQ2S^*}$ or $k_{IL,^3CDOM^*} = 0.05 k_{IL,^3AQ2S^*}$ in different sets of calculations.

Because depth and dissolved organic carbon (DOC) are the water body features that most influence photochemical reactions (Vione et al., 2014), the ILs half-life times were computed as a function of these two variables. Reasonable values were assumed for other water parameters of photochemical significance, *i.e.*, 0.1 mM nitrate, 1 μ M nitrite, 1 mM bicarbonate, and 10 μ M carbonate (Vione et al., 2014). On this basis and for fair-weather summertime irradiation, APEX returned the half-life

times reported in **Figure 3** (**3A,D: BMPOTFB; 3B,E: EPTFB; 3C,F: CPPC; 3A,B,C:** $k_{IL,^3CDOM^*} = k_{IL,^3AQ2S^*}$; **3D,E,F:** $k_{IL,^3CDOM^*} = 0.05 k_{IL,^3AQ2S^*}$). First of all, note that all the half-life times

increase with increasing depth and that they also increase with DOC, with the partial exception of a trend with a maximum (**EPTFB** with $k_{EPTFB,^3CDOM^*} = k_{EPTFB,^3AQ2S^*}$, see **Figure 3B**). The rationale of

the depth trend is that the lower depths of deep water bodies are poorly illuminated by sunlight, a phenomenon that offsets the elevated photoreactivity at the water surface. Increasing DOC means

increasing DOM and CDOM. The occurrence of CDOM inhibits the direct photolysis (due to competition for irradiance between CDOM and the substrate(s)), while DOM causes an even larger

inhibition of the $\bullet OH/CO_3^{\bullet -}$ reactions (due to scavenging of the radicals) (Vione et al., 2014). The inhibition of direct photolysis, of $\bullet OH$ and $CO_3^{\bullet -}$ processes is often not offset by the enhancement

of the reactions triggered by $^3CDOM^*$ and 1O_2 , of which CDOM is the only source. Actually, CDOM tends to reach absorption saturation in deep waters with high DOC, in which case the

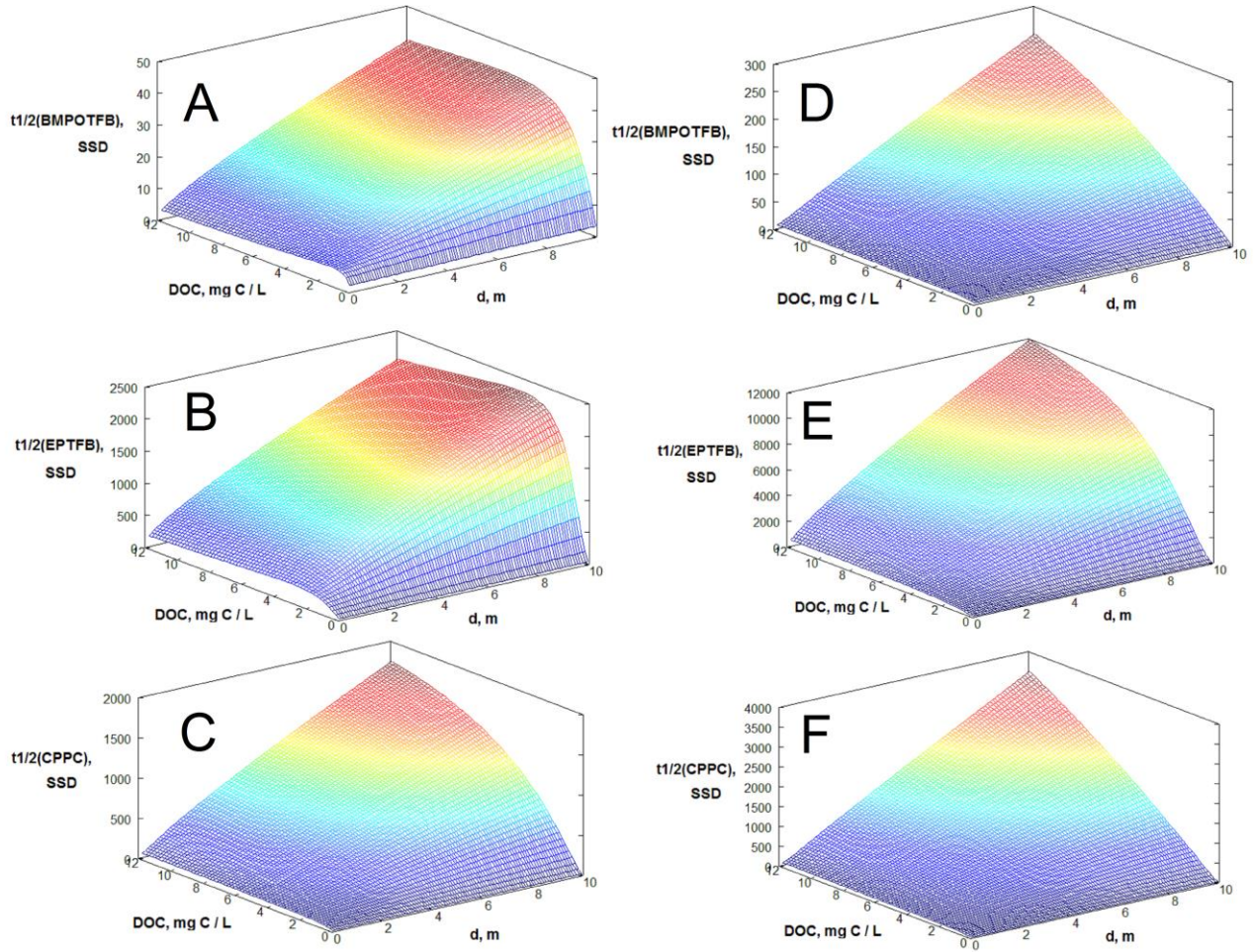
production of $^3CDOM^*$ is little enhanced by a CDOM increase. In contrast, the scavenging of $\bullet OH/CO_3^{\bullet -}$ and the competition for irradiance do not undergo saturation effects (Avetta et al.,

2016). There are some exceptions, however: if the reactivity of a substrate with $^3\text{CDOM}^*/^1\text{O}_2$ is remarkably high, these processes can significantly increase the degradation kinetics at elevated DOC. In this case one can observe a maximum in the half-life times as a function of the DOC (Fabbri et al., 2015), which happened here with **EPTFB** if $k_{\text{EPTFB}^3\text{CDOM}^*} = k_{\text{EPTFB}^3\text{AQ2S}^*}$ (**Figure 3B**).

Among the studied ILs, **BMPOTFB** is predicted to be by far the most photolabile compound in the natural environment. This prediction follows the results of the irradiation experiments, which already suggested that **BMPOTFB** was more photoreactive than **EPTFB** or **CPPC** via both direct photolysis and indirect photochemistry. If $k_{\text{BMPOTFB}^3\text{CDOM}^*} = k_{\text{BMPOTFB}^3\text{AQ2S}^*}$, phototransformation would be an important attenuation pathway for **BMPOTFB** under all the water conditions considered in **Figure 3** (depth = 0-10 m, DOC = 0-12 mg C L⁻¹). If $k_{\text{BMPOTFB}^3\text{CDOM}^*} = 0.05 k_{\text{BMPOTFB}^3\text{AQ2S}^*}$, the photodegradation half-life times would be quite long in deep and high-DOC waters. When considering the half-life time data reported in **Figure 3**, it should be noted that one cannot have year-long fair-weather summertime conditions in mid-latitude environments. Therefore, the longer lifetimes are certainly underestimated.

Differently from **BMPOTFB**, the predicted photochemical half-life times of **EPTFB** and **CPPC** are very high and they can reach years to decades in deep water bodies with high DOC. Under such circumstances, other processes will prevail over phototransformation in the environmental attenuation of these ILs. Photochemistry could still play some role for **EPTFB** and **CPPC**, but only in water bodies that are shallow and have low DOC at the same time.

344



345

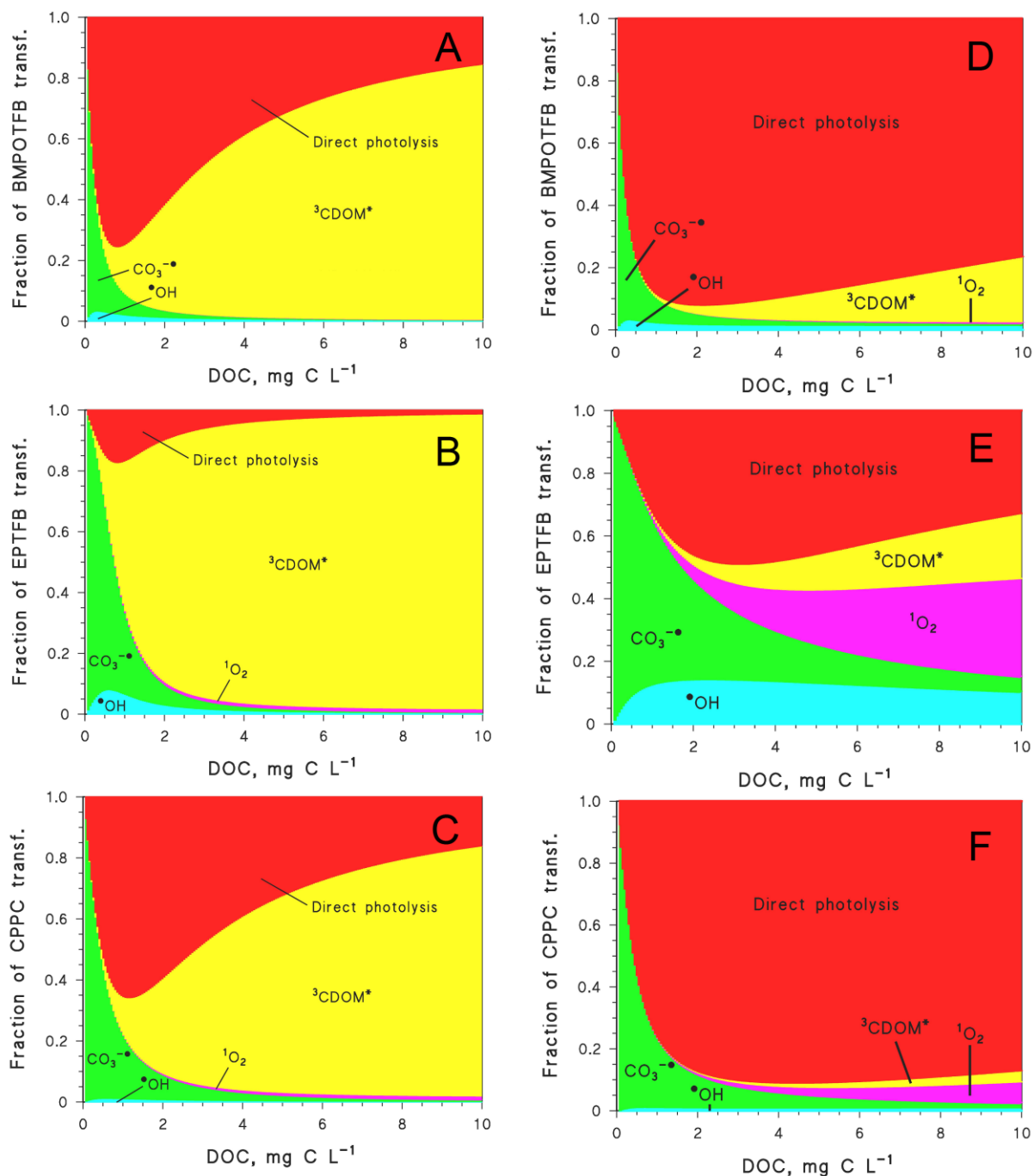
346

347 **Figure 3.** Half-life times predicted by APEX (SSD = summer sunny days equivalent to fair-weather
 348 15 July at 45°N latitude), as a function of the DOC and the water depth d , for: (A) **BMPOTFB**,
 349 with $k_{BMPOTFB^3CDOM^*} = k_{BMPOTFB^3AQ2S^*}$; (B) **EPTFB**, with $k_{EPTFB^3CDOM^*} = k_{EPTFB^3AQ2S^*}$; (C) **CPPC**, with
 350 $k_{CPPC^3CDOM^*} = k_{CPPC^3AQ2S^*}$; (D) **BMPOTFB**, with $k_{BMPOTFB^3CDOM^*} = 0.05 k_{BMPOTFB^3AQ2S^*}$; (E) **EPTFB**,
 351 with $k_{EPTFB^3CDOM^*} = 0.05 k_{EPTFB^3AQ2S^*}$; (F) **CPPC**, with $k_{CPPC^3CDOM^*} = 0.05 k_{CPPC^3AQ2S^*}$. Other water
 352 conditions: 0.1 mM nitrate, 1 μ M nitrite, 1 mM bicarbonate, 10 μ M carbonate.

353

354 **Figure 4** reports, as a function of the DOC, the fractions of ILs phototransformation that are
 355 accounted for by the different photoreaction pathways, for a water depth of 5 m and other
 356 conditions as per the above discussion (**4A,D: BMPOTFB**; **4B,E: EPTFB**; **4C,F: CPPC**; **4A,B,C:**
 357 $k_{IL, {}^3CDOM^*} = k_{IL, {}^3AQ2S^*}$; **4D,E,F:** $k_{IL, {}^3CDOM^*} = 0.05 k_{IL, {}^3AQ2S^*}$). The model predicts that the reactions with
 358 $CO_3^{\cdot-}$ can be important for all ILs at low DOC (usually below 2 mg C L⁻¹), while $\cdot OH$ and 1O_2 can
 359 be important only in the case of **EPTFB**. The reactions with ${}^3CDOM^*$ can be major pathways at
 360 high DOC if $k_{IL, {}^3CDOM^*} = k_{IL, {}^3AQ2S^*}$, while they become secondary processes if
 361 $k_{IL, {}^3CDOM^*} = 0.05 k_{IL, {}^3AQ2S^*}$. In the latter case, the direct photolysis is expected to strongly dominate the
 362 phototransformation of both **BMPOTFB** and **CPPC**.
 363 By crossing these results with the half-life time data, which show the environmental water
 364 conditions where photochemistry can be important in IL attenuation, one gets that: (i) the direct
 365 photolysis is very relevant for **BMPOTFB**, especially in water bodies where the occurrence of
 366 CDOM of mainly aquatic origin would limit the triplet-sensitized processes. Other significant
 367 **BMPOTFB** transformation pathways are $CO_3^{\cdot-}$ at low DOC and possibly ${}^3CDOM^*$ at high DOC,
 368 in the presence of significant amounts of soil-derived organic matter that would enhance the
 369 reactions of triplet sensitization (De Laurentiis et al., 2012); (ii) the photodegradation of **EPTFB**
 370 may only be significant in low-DOC waters, and in these conditions the prevailing pathways are the
 371 direct photolysis and the reactions with $\cdot OH$ and $CO_3^{\cdot-}$. The exact value of $k_{EPTFB, {}^3CDOM^*}$ is of
 372 limited interest because, for the ${}^3CDOM^*$ processes to play a significant role, one needs relatively
 373 high-DOC conditions where **EPTFB** photochemistry cannot be important; (iii) a similar issue holds
 374 for **CPPC**, although in this case the $\cdot OH$ process can be neglected and the only important low-DOC
 375 pathways are the direct photolysis and the $CO_3^{\cdot-}$ reaction.

376



377

378 **Figure 4.** Fractions of ILs phototransformation accounted for by the different photoinduced
 379 pathways, as predicted by the APEX software for summertime irradiation conditions. **(A)**
 380 **BMPOTFB**, with $k_{BMPOTFB^3CDOM^*} = k_{BMPOTFB^3AQ2S^*}$; **(B) EPTFB**, with $k_{EPTFB^3CDOM^*} = k_{EPTFB^3AQ2S^*}$; **(C)**
 381 **CPPC**, with $k_{CPPC^3CDOM^*} = k_{CPPC^3AQ2S^*}$; **(D) BMPOTFB**, with $k_{BMPOTFB^3CDOM^*} = 0.05 k_{BMPOTFB^3AQ2S^*}$;
 382 **(E) EPTFB**, with $k_{EPTFB^3CDOM^*} = 0.05 k_{EPTFB^3AQ2S^*}$; **(F) CPPC**, with $k_{CPPC^3CDOM^*} = 0.05 k_{CPPC^3AQ2S^*}$.
 383 Other water conditions: 5 m depth, 0.1 mM nitrate, 1 μ M nitrite, 1 mM bicarbonate, 10 μ M
 384 carbonate.

3.3. ILs toxicity assessment upon photoinduced degradation

Acute toxicity was monitored over time upon UVB direct photolysis of the studied ILs. The choice of the direct photolysis pathway for the toxicity study has two reasons: (i) experimental simplicity, because the assessment of toxicity in indirect phototransformation is complicated by the possible production of toxic species/intermediates from the photosensitizers (De Luis et al., 2010). The indirect phototransformation processes might be incompletely accounted for in control experiments carried out without the substrates, because the substrates themselves are major scavengers of transient species (e.g. in the case of $\bullet\text{OH}$ and $\text{CO}_3^{\bullet-}$), and the transient steady-state concentrations may vary dramatically when the substrates are absent; (ii) environmental significance. The direct photolysis is an important process in the phototransformation of **BMPOTFB**, for which photochemistry may be a significant attenuation pathway in surface waters. The direct photolysis is less important for **EPTFB** (see **Figure 4**), but the phototransformation kinetics of this compound are predicted to be very slow except for low-DOC waters (**Figure 3**). In these conditions, the direct phototransformation pathway could play a remarkable role. The phototransformation of **CPPC** can only be significant under low-DOC conditions, where the direct photolysis is an important degradation pathway.

The acute toxicity tests were carried out by monitoring changes in the natural emission of the luminescent bacteria *Vibrio fischeri*, when exposed to potentially toxic compounds. Out of the various available bioassays, this test is sensitive, rapid, cost-effective, reproducible, and it can be used for almost all kinds of toxic compounds (Parvez et al., 2006, Matsushita et al., 2015). The toxicity is here expressed as the percentage of inhibition of the bacteria luminescence. Results obtained on samples subjected to different irradiation times are plotted in **Figure 5** (**5A**: time trend of ILs in the irradiated solutions; **5B**: time trend of the toxicity in the same solutions). The studied ILs are not toxic, as shown by the absence or near absence of a toxic effect before irradiation. Under UVB light the photoinduced transformation of **EPTFB** proceeded through the formation of almost

harmless TPs, and a slight toxicity increase was only observed after 7 days of irradiation. Unfortunately, this compound is the studied IL for which phototransformation (either direct or indirect) is expected to play the least important role in the natural environment (see **Figure 3**). In contrast, the toxicity of irradiated **CPPC** and **BMPOTFB** increased over time, thereby suggesting that their phototransformation proceeded through the formation of moderately toxic compounds.

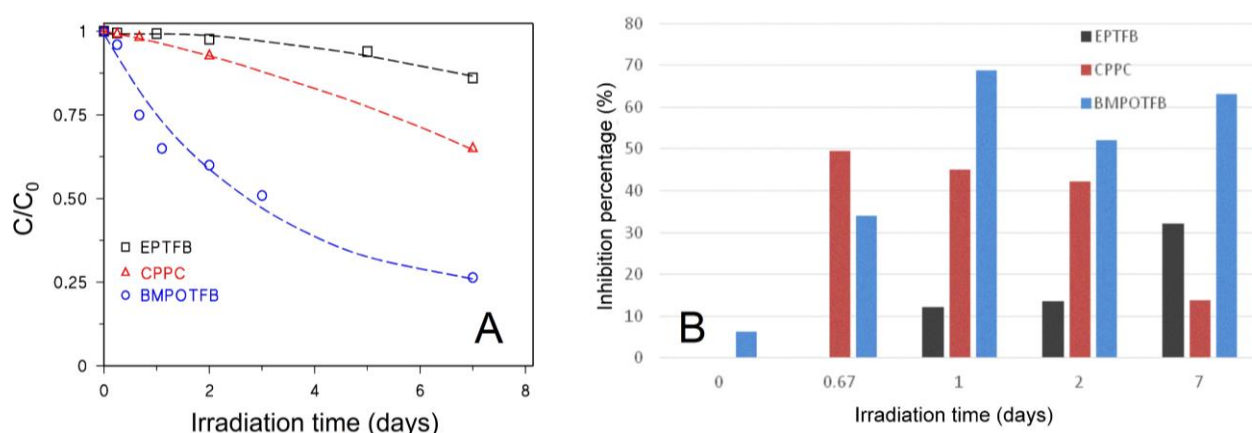


Figure 5. (A) Time trends of **BMPOTFB**, **EPTFB** and **CPPC** (20 mg L⁻¹ initial loading in separate solutions) upon direct photolysis under UVB irradiation. **(B)** Toxicity evolution (inhibition of *Vibrio fischeri* emission) in the same irradiated solutions shown in the (A) panel.

3.4. Characterization of the transformation products

The direct photolysis of **EPTFB**, **CPPC** and **BMPOTFB** yielded several transformation products (TPs), which were detected in ESI positive mode *via* HPLC-HRMS. **Tables SM2-SM4** in the SM report the measured m/z ratios and the most probable empirical formulas for all the detected TPs. The relevant time evolution profiles are provided in **Figure 6**. Among the TPs of **BMPOTFB**, a few of them were formed at early reaction times and disappeared during the course of the irradiation experiments, which lasted for up to eight days. Several other TPs appeared at relatively long

429 irradiation times, and their concentration increased during irradiation. The various TPs could be
430 formed upon direct photolysis through three different pathways shown in **Scheme 1** and involving:
431 (*a*) hydroxylation; (*b*) detachment/shortening of the butyl chain; (*c*) double bond formation.

432 The MS² spectrum of **BMPOTFB** has a product ion at 94.0652 *m/z*, presumably produced by the
433 loss of the butyl chain (see **Table SM2**). This peculiar loss was helpful in attributing the structures
434 of unknown TPs. A TP having 166.1233 *m/z* (**TP-166**) is consistent with a monohydroxyderivative.
435 The formation of a product ion at 71.0447 *m/z* (hydroxylated butyl moiety) in the MS² spectrum of
436 **TP-166**, combined with the loss of C₂H₆, permits to locate the OH group on the butyl chain and to
437 confine it on C1 or C2.

438 Four species with 164.1077 *m/z* (**TP-164A** through **D**) were detected and attributed to keto
439 derivatives. For **TP-164A** it was not possible to acquire enough structural information, while for the
440 other compounds the presence of the product ion at 94.0634 *m/z* allows the placement of the
441 hydroxyl group on the butyl chain. Additionally, **TP-164B** presents the structural diagnostic loss of
442 formaldehyde that allows the keto group to be located on C4 (McLafferty and Turecek, 1993).

443 Three species with 182.1184 *m/z* (**TP-182A** through **C**) are consistent with **BMPOTFB**
444 dihydroxyderivatives. All these TPs show the product ion at 94.0652 *m/z* in their MS² spectrum,
445 thereby allowing the two OH groups to be located on the butyl chain. **TP-182C** should have one
446 OH group on the C4 atom of the butyl chain, as suggested by the loss of methanol.

447 Three species with 180.0995 *m/z* (**TP-180A** through **C**) should be dihydroxylated/oxidized
448 compounds. In the case of **TP-180C**, the loss of formic acid and the formation of the precursor ion
449 at 94.0634 *m/z* suggest the presence of a carboxylic group on the butyl chain.

450

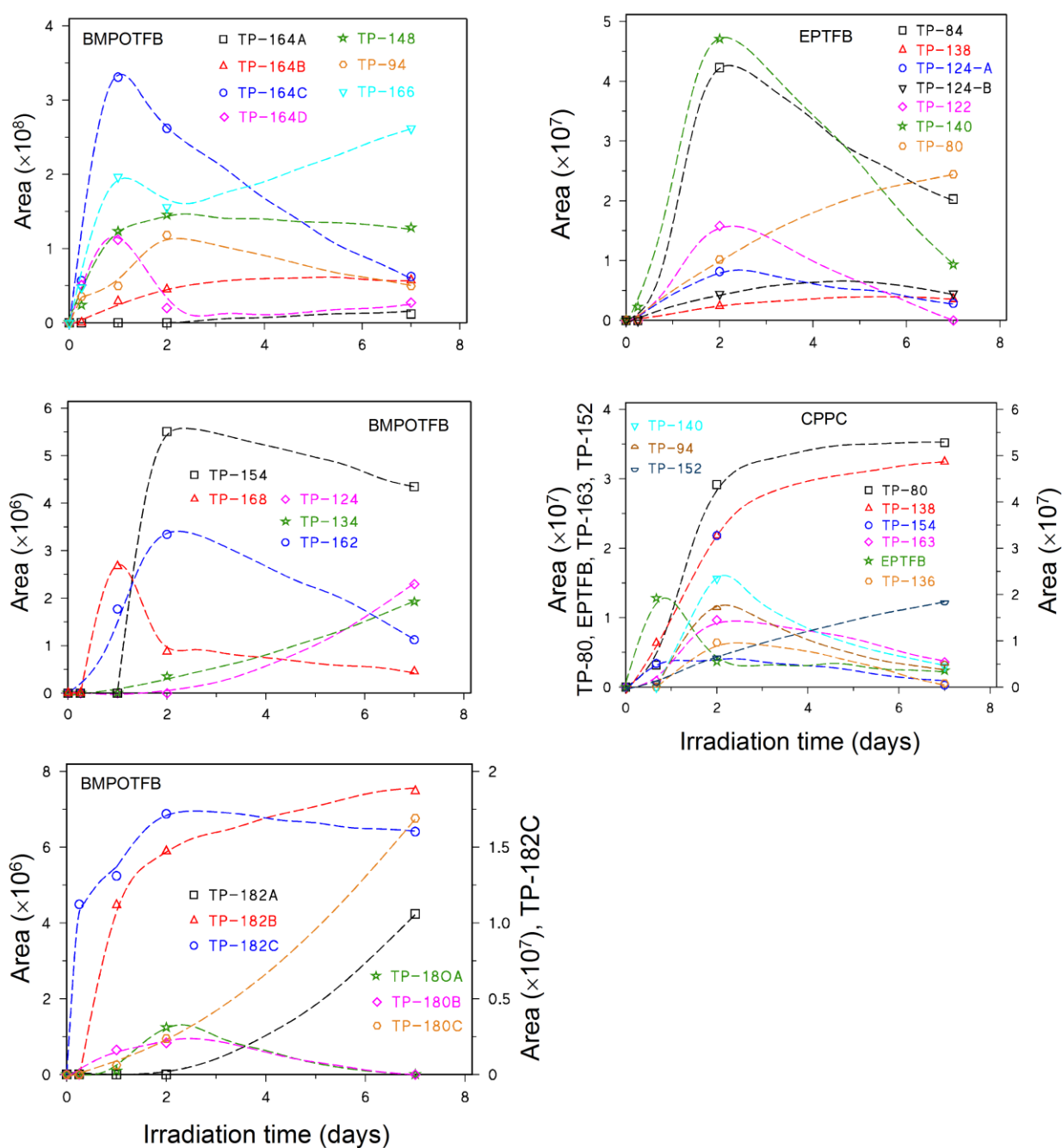
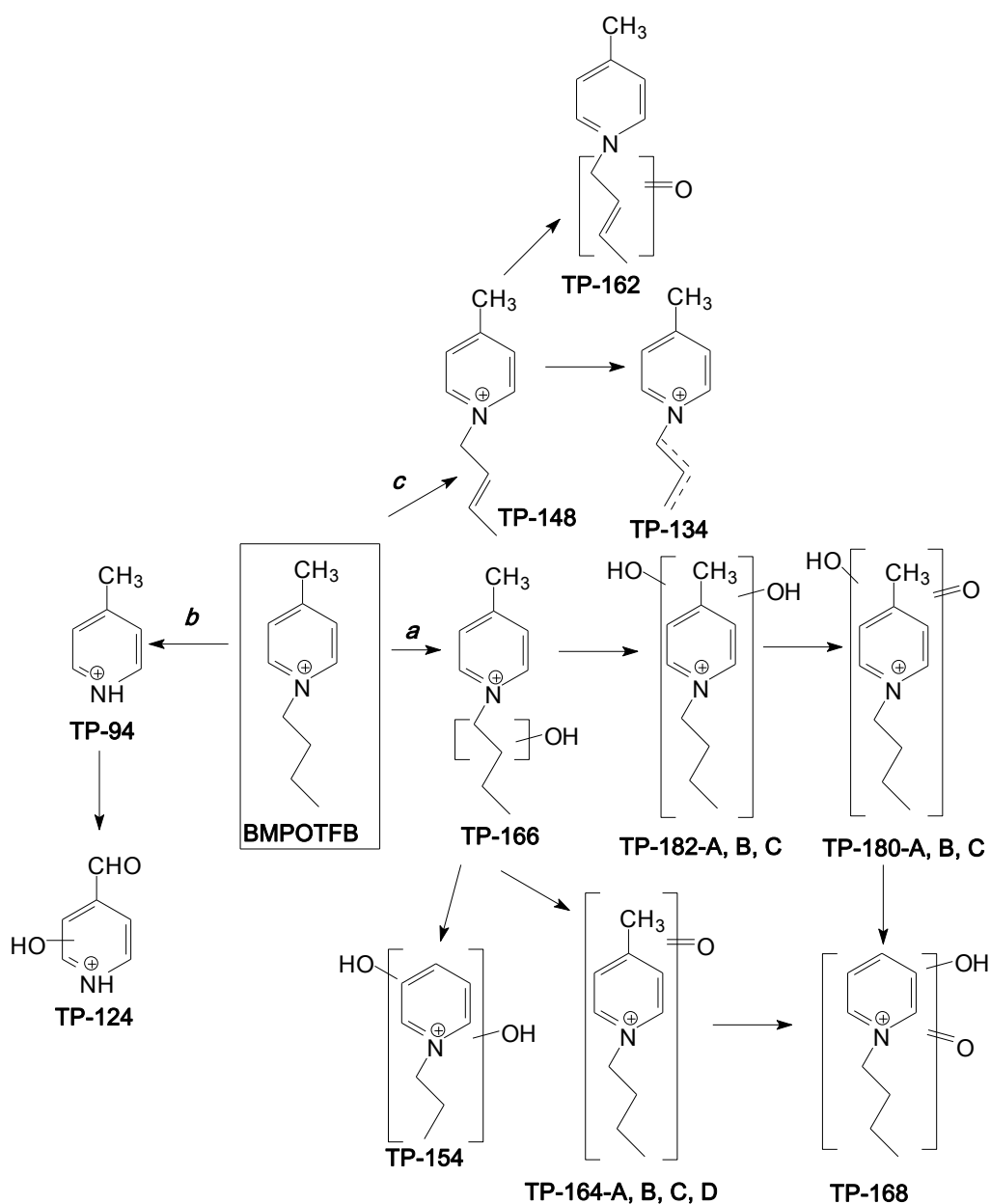


Figure 6. Time evolution of the TPs formed upon UVB irradiation of (left side) **BMPOTFB** and of (right side) **EPTFB** (top) and **CPPC** (bottom). Multiple plots are provided for **BMPOTFB** to show TPs with different peak areas, and for readability issues as well. The dashed curves are just a guide for the eye. In a couple of cases data are plotted against different Y-axes, located on the right hand and on the left hand of each plot. The least numerous group of compounds is listed on the given axis. The remaining compounds, not explicitly mentioned, are plotted against the other axis.



458

459 **Scheme 1.** Proposed transformation pathways followed by **BMPOTFB** under direct photolysis.

460

461 Three compounds at 162.0891, 148.1126 and 134.0967 m/z with empirical formulas $C_{10}H_{12}ON$,
 462 $C_{10}H_{14}ON$ and $C_9H_{12}N$, respectively, are consistent with progressive dealkylation and with
 463 formation of a double bond on the alkyl chain. For **TP-162**, the most abundant ion in MS^2 exhibits a
 464 C_4H_6O loss that suggests the occurrence of a keto group on the butyl chain.

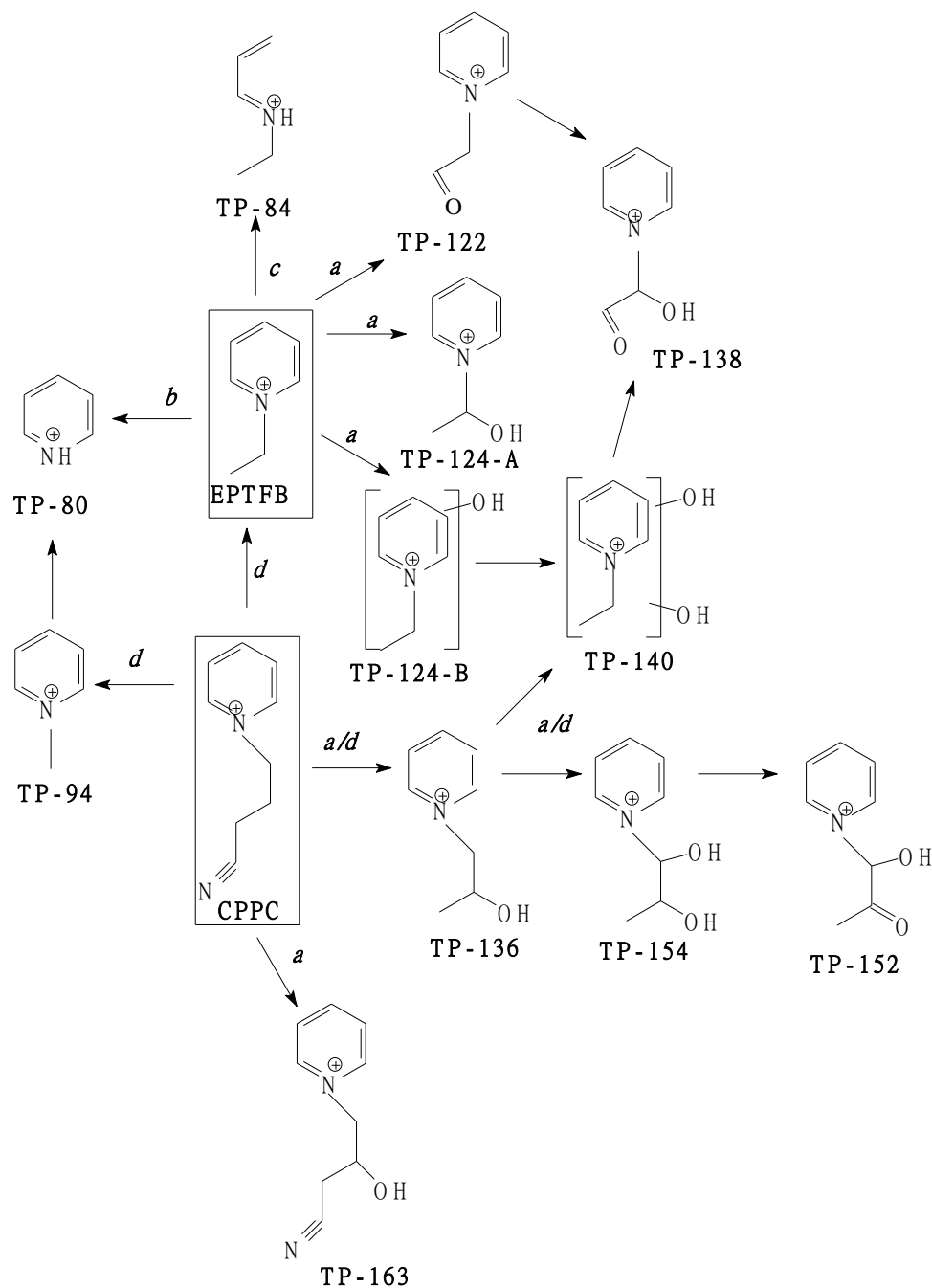
465 **TP-168** and **TP-154** may be formed *via* the detachment of a methyl group and/or *via* side-chain
466 shortening, but insufficient mass information was available to propose a univocal structure.

467 **TP-94** and **TP-124** are formed upon detachment of the butyl chain. **TP-94** is consistent with 4-
468 methylpyridine, while **TP-124** would involve methyl oxidation and possibly ring hydroxylation.
469 Unfortunately, the information contained in the MS spectra did not allow for the proposal of a
470 proper location for the OH group in **TP-124**.

471 As far as the indirect photochemistry processes are concerned, **TP-148** was also detected upon
472 reactions with $\bullet\text{OH}$, $\text{CO}_3^-\bullet$ and $^3\text{AQ2S}^*$, **TP-164 B,D** with $\bullet\text{OH}$, **TP-164 C,D** and **TP-166 C,D** with
473 $^3\text{AQ2S}^*$, and **TP-94** with $\text{CO}_3^-\bullet$. The formation of partially overlapping TPs in different pathways
474 is quite common in phototransformation reactions (De Laurentiis et al., 2014).

475 In the case of **EPTFB**, three main transformation pathways could be detected under direct
476 photolysis conditions. These pathways involve: (*a*) hydroxylation; (*b*) detachment of the ethyl
477 chain, and (*c*) ring opening (see **Scheme 2**). The MS^2 spectrum of **EPTFB** has the ion at 80.0492
478 m/z as base peak, formed through the detachment of the ethyl chain (C_2H_4 , see **Table SM3**). Upon
479 photolysis, pathway *a* likely yields two isobaric species with 124.0757 m/z and empirical formula
480 $\text{C}_7\text{H}_{10}\text{ON}$, which can be attributed to hydroxyderivatives. In the case of **TP-124A**, the loss of
481 $\text{C}_2\text{H}_4\text{O}$ in the MS^2 spectrum suggests that the OH substituent occurs on the alkyl chain. Moreover,
482 the absence of methanol loss tentatively suggests that OH is located on the ethyl carbon atom bound
483 to nitrogen (C1). For **TP-124B**, the absence of MS^2 product ions prevented any hypothesis
484 concerning the OH position. The formation of **TP-122**, with empirical formula $\text{C}_7\text{H}_8\text{ON}$, likely
485 involved the oxidation of the alcoholic group to a keto one. The loss of C_2HON in the MS^2
486 spectrum supports the occurrence of a keto group on the alkyl chain, which should be located on C2
487 as suggested by the CO loss (McLafferty and Turecek, 1993). Pathway *a* also involved the
488 formation of TPs with empirical formula $\text{C}_7\text{H}_{10}\text{O}_2\text{N}$ (**TP-140**) and $\text{C}_7\text{H}_8\text{O}_2\text{N}$ (**TP-138**), which are

489 well-matched with dihydroxylated and dihydroxylated/oxidized derivatives, respectively. However,
 490 the absence of MS² product ions prevented any hypothesis about the location of the two OH groups.
 491



492
 493 **Scheme 2.** Proposed transformation pathways followed by compounds **EPTFB** and **CPPC** upon
 494 direct photolysis.

495

Further transformation (pathway *b*) involved the detachment of the alkyl chain with formation of pyridine (**TP-80**). An alternative route (pathway *c*) would proceed through ring opening to yield compound **TP-84**. The most abundant compounds (as far as peak areas are concerned) were **TP-140**, **TP-84** and **TP-80**, thereby suggesting that the three pathways had similar importance. Interestingly, the compound **TP-84** was also detected upon reactions with $\bullet\text{OH}$, $\text{CO}_3^{\bullet-}$ and $^3\text{AQ2S}^*$, and **TP-140** upon reaction with $\bullet\text{OH}$ as well.

In a close analogy with **EPTBF**, the MS^2 spectrum of **CPPC** presents as base peak the pyridinium ion at 80.0492 m/z . This ion is likely formed through the detachment of the cyano-propyl chain (see **Table SM4**). The direct photolysis of **CPPC** involved hydroxylation (see pathway *a* in **Scheme 2**). **TP-163** is well-matched with a monohydroxylated derivative, and the detected MS^2 product ions are consistent with losses of $\text{C}_2\text{H}_3\text{N}$ and $\text{C}_3\text{H}_3\text{ON}$. Therefore, the OH substituent should not occur on the cyano carbon (C4) or on the carbon attached to the cyano group (C3) (McLafferty and Turecek, 1993). The occurrence of OH on the carbon atom bound to the ring nitrogen (C1) also looks little likely, leaving C2 as the most reasonable position for the OH group. The MS data are also consistent with chain shortening (pathway *d*) and with a combined chain shortening/hydroxylation (pathway *a/d*). The detachment of the methylcyano group accounts for the formation of a compound with 108.0809 m/z , recognized as **EPTFB** and confirmed by standard match. A further chain shortening would produce **TP-94**, which was identified as 1-methylpyridine. The latter could yield **TP-80**, matched with pyridine (also detected during **EPTFB** photolysis), through detachment of the methyl group. Pathway *a/d* yields **TP-136**, **TP-154** and **TP-152** through cyano group detachment and hydroxylation. In all cases, the OH groups were added to the propyl chain as assessed by the product ion at 80.0478 m/z (pyridinium ion) in the relevant MS^2 spectra. The presence of some structurally-diagnostic ions allowed a univocal location of the oxygen atoms on the alkyl chain. **TP-136** formation would imply the detachment of the cyano group and the

520 oxidation of the alkyl chain. Actually, the absence of formaldehyde loss combined with C_2H_2O and
521 C_3H_4O losses allowed the location of the keto group on C2.

522 Based on its exact mass, **TP-152** might have an OH group and a keto one. The oxygen-containing
523 functions should be both located on the alkyl chain, as suggested by the occurrence of the
524 pyridinium ion in the MS^2 spectrum. The absence of any methanol loss is not consistent with the
525 occurrence of OH on C3. Together with the loss of ketene, this suggests that the keto group should
526 be located on C2 and the hydroxyl one on C1. Therefore, **TP-152** could be tentatively identified as
527 the oxidized form of **TP-154**. The formation of **TP-138** and **TP-140** likely involved methylcyano-
528 group detachment and hydroxylation. The retention times and fragmentation spectra of the TPs
529 derived from **CPPC** matched well with the TPs formed from **EPOTFB** photolysis. As far as peak
530 areas are concerned, the main TPs were **TP163**, formed through pathway *a*, **TP108** and **TP80**,
531 involving pathway *d*. While **EPOTFB** was formed from **CPPC** at early reaction times and reached its
532 maximum concentration after 1 day of irradiation, all the other TPs were more persistent and either
533 peaked at two days irradiation, or continued accumulating up to at least eight days. No TPs were
534 detected upon indirect phototransformation of **CPPC**, probably because of the scarce reactivity of
535 this substrate with the studied transient species.

536 The occurrence of definite chemical functions allows some hypotheses to be advanced concerning
537 the potential toxicity of TPs (Mayo-Bean et al., 2012). On this basis and from the above discussion
538 one may assume that among the detected TPs of **BMPOTFB**, those for which a univocal chemical
539 structure could be proposed are unlikely to be more toxic than the parent compound, because no
540 potentially toxic functionalities were added (Mayo-Bean et al., 2012). A toxicity increase could be
541 expected in the (possible but not confirmed) circumstance that dihydroxylation involved the
542 aromatic ring, especially if two OH groups occurred in para position (hydroquinone derivatives)
543 (Mayo-Bean et al., 2012). Similar considerations hold for **CPPC** and **EPOTFB**.

544

545 4. Conclusions

- 546 • Phototransformation in sunlit surface waters is a potentially important attenuation pathway for
547 **BMPOTFB** but not for **EPTFB** and **CPPC**, with the possible exception of shallow water
548 bodies with very low DOC.
- 549 • The phototransformation of **BMPOTFB** is expected to proceed through $\text{CO}_3^{\cdot-}$ reactions at
550 low DOC and *via* direct photolysis at higher DOC. In water bodies that are rich in pedogenic
551 organic matter (humic and fulvic substances), also the $^3\text{CDOM}^*$ reactions could play an
552 important role at elevated DOC.
- 553 • The phototransformation of **EPTFB** and **CPPC** is extremely slow in high-DOC waters, thus
554 the most relevant photochemical attenuation pathways (provided that the water body is
555 shallow) are those prevailing at low DOC: $\text{CO}_3^{\cdot-}$, direct photolysis and, for **EPTFB** alone,
556 $\cdot\text{OH}$.
- 557 • The direct photolysis of **BMPOTFB** and **CPPC** yields TPs that are more toxic than the parent
558 compound. The main identified reaction pathways upon direct photolysis are hydroxylation,
559 lateral-chain shortening and ring opening, and toxic TPs might be formed by multiple
560 hydroxylation if this process yields hydroquinone-like derivatives.

562 Acknowledgments

563 We acknowledge support by MIUR, in the frame of the collaborative international consortium
564 WATERJPI2013-MOTREM of the "Water Challenges for a Changing World" Joint Programming
565 Initiative (WaterJPI) Pilot Call.

566

567 **References**

- 568 Avetta, P., Fabbri, D., Minella, M., Brigante, M., Maurino, V., Minero, C., Pazzi, M., Vione, D.,
569 2016. Assessing the phototransformation of diclofenac, clofibric acid and naproxen in surface
570 waters: Model predictions and comparison with field data. *Water. Res.* 105, 383-394.
- 571 Bandres, I., Giner, B., Artigas, H., Royo, F. M., Lafuente, C., 2008. Thermophysic comparative
572 study of two isomeric pyridinium-based ionic liquids. *J. Phys. Chem. B* 112, 3077-3084.
- 573 Bahn Müller, S., von Gunten, U., Canonica, S., 2014. Sunlight-induced transformation of
574 sulfadiazine and sulfamethoxazole in surface waters and wastewater effluents. *Water Res.* 57,
575 183-192.
- 576 Bedini, A., De Laurentiis, E., Sur, B., Maurino, V., Minero, C., Brigante, M., Mailhot, G., Vione,
577 D., 2012. Phototransformation of anthraquinone-2-sulphonate in aqueous solution.
578 *Photochem. Photobiol. Sci.* 11, 1445-1453.
- 579 Bintou, A. T., Bianco, A., Mailhot, G., Brigante, M., 2015. A new insight into ethoxyquin fate in
580 surface waters: Stability, direct and indirect photochemical behaviour and the identification of
581 main products. *J. Photochem. Photobiol. A: Chem.* 311, 118-126.
- 582 Bodrato, M., Vione, D., 2014. APEX (Aqueous Photochemistry of Environmentally occurring
583 Xenobiotics): A free software tool to predict the kinetics of photochemical processes in
584 surface waters. *Environ. Sci.: Processes Impacts* 16, 732-740.
- 585 Braslavsky, S.E., 2007. Glossary of terms used in photochemistry. third edition. *Pure Appl. Chem.*
586 79, 293-465.
- 587 Bubalo, M.C.; Radošević, K.; Redovniković, I.R.; Halambek, J.; Srček, V.G., 2014. A brief
588 overview of the potential environmental hazards of ionic liquids, *Ecotoxicol. Environ. Saf.*,
589 2014,99,1-12.

590 Buxton, G. V., Greenstock, C. L., Helman, W. P., Ross, A. B., 1988. Critical review of rate
 591 constants for reactions of hydrated electrons, hydrogen atoms and hydroxyl radicals ($\bullet\text{OH}/\text{O}^-\bullet$)
 592 in aqueous solution. *J. Phys. Chem. Ref. Data* 17, 513-886.

593 Calza, P., Vione, D., Fabbri, D., Aigotti, R., Medana, C., 2015. Imidazolium-based ionic liquids in
 594 water: Assessment of photocatalytic and photochemical transformation. *Environ. Sci.*
 595 *Technol.* 49, 10951-10958.

596 Canonica, S., Kohn, T., Mac, M., Real, F.J., Wirz, J., von Gunten, U., 2005. Photosensitizer method
 597 to determine rate constants for the reaction of carbonate radical with organic compounds.
 598 *Environ. Sci. Technol.* 39, 9182-9188.

599 Chiwa, M., Higashi, N., Otsuki, K., Kodama, H., Miyajima, T., Takeda, K., Sakugawa, H., 2015.
 600 Sources of hydroxyl radical in headwater streams from nitrogen-saturated forest.
 601 *Chemosphere* 119, 1386-1390.

602 Czerwicka, M., Stolte, S., Müller, A., Siedlecka, E. M., Gołebiowski, M., Kumirska J., Stepnowski,
 603 P., 2009. Identification of ionic liquid breakdown products in an advanced oxidation system.
 604 *J. Hazard. Mater.* 171, 478-483.

605 Dantas, R. F., Canterino, M., Marotta, R., Sansa, C., Esplugas, S., Andreozzi, R., 2007. Bezafibrate
 606 removal by means of ozonation: Primary intermediates, kinetics, and toxicity assessment.
 607 *Water Res.* 41, 2525-2532.

608 De Laurentiis, E., Minella, M., Maurino, V., Minero, C., Brigante, M., Mailhot, G., Vione, D.,
 609 2012. Photochemical production of organic matter triplet states in water samples from
 610 mountain lakes, located below or above the tree line. *Chemosphere* 88, 1208-1213.

611 De Laurentiis, E., Prasse, C., Ternes, T.A., Minella, M., Maurino, V., Minero, C., Sarakha, M.,
 612 Brigante, M., Vione, D., 2014. Assessing the photochemical transformation pathways of

613 acetaminophen relevant to surface waters: transformation kinetics, intermediates, and
614 modelling. *Water Res.* 53, 235-248.

615 De Luis, A. M., Lombrana, J. I., Menendez, A., Sanz, J., 2011. Analysis of the toxicity of phenol
616 solutions treated with H₂O₂/UV and H₂O₂/Fe oxidative systems. *Ind. Eng. Chem. Res.* 50,
617 1928-1937.

618 Dong, M. M., Trenholm, R., Rosario-Ortiz, F. L., 2015. Photochemical degradation of atenolol,
619 carbamazepine, meprobamate, phenytoin and primidone in wastewater effluents. *J. Hazard.*
620 *Mater.* 2015, 282, 216-223.

621 Fabbri, D., Minella, M., Maurino, V., Minero, C., Vione, D., 2015. Photochemical transformation
622 of phenylurea herbicides in surface waters: A model assessment of persistence, and
623 implications for the possible generation of hazardous intermediates. *Chemosphere* 119, 601-
624 607.

625 Frank, R., Klöpffer, W., 1988. Spectral solar photo irradiance in Central Europe and the adjacent
626 north Sea, *Chemosphere* 17, 985-994.

627 Giannakis, S., Polo Lopez, M. I., Spuhler, D., Sanchez Perez, J. A. Fernandez Ibanez, P., Pulgarin,
628 C., 2016a. Solar disinfection is an augmentable, in situ-generated photo-Fenton reaction-Part
629 1: A review of the mechanisms and the fundamental aspects of the process. *Appl. Catal. B:*
630 *Environ.* 199, 199-223.

631 Giannakis, S., Polo Lopez, M. I., Spuhler, D., Sanchez Perez, J. A. Fernandez Ibanez, P., Pulgarin,
632 C., 2016b. Solar disinfection is an augmentable, in situ-generated photo-Fenton reaction Part
633 2: A review of the applications for drinking water and wastewater disinfection. *Appl. Catal. B:*
634 *Environ.* 198, 431-446.

635 Guerrero, H., Garcia-Mardones, M., Cea, P., Lafuente, C., Bandres, I., 2012. Correlation of the
 636 volumetric behaviour of pyridinium-based ionic liquids with two different equations.
 637 *Thermochim. Acta* 531, 21-27.

638 Herrmann, H., Hoffmann, D., Schaefer, T., Bräuer, P., Tilgner, A., 2010. Tropospheric aqueous-
 639 phase free-radical chemistry: Radical sources, spectra, reaction kinetics and prediction tools.
 640 *ChemPhysChem* 11, 3796-3822.

641 Holbrey J. D., Seddon K. R., 1999. Ionic liquids. *Clean Technol. Environ.* 1, 223-236.

642 Huang, J. P., Mabury, S. A., 2000. Steady-state concentrations of carbonate radicals in field waters.
 643 *Environ. Toxicol. Chem.* 19, 2181-2188.

644 Katsoyiannis, I. A., Canonica, S., von Gunten, U., 2011. Efficiency and energy requirements for the
 645 transformation of organic micropollutants by ozone, O_3/H_2O_2 and UV/ H_2O_2 . *Water Res.* 45,
 646 3811-3822.

647 Keen, O. S., McKay, G., Mezyk, S. P., Linden, K. G., Rosario-Ortiz, F. L., 2014. Identifying the
 648 factors that influence the reactivity of effluent organic matter with hydroxyl radicals. *Water*
 649 *Res.* 50, 408-419.

650 Kralisch, D., Stark, A., Korsten, S., Kreisel G., Ondruschka, B., 2005. Energetic, environmental and
 651 economic balances: Spice up your ionic liquid research efficiency. *Green Chem.* 7, 301-309.

652 Janssen, E. M. L., Erickson, P. R., McNeill, K., 2014. Dual roles of dissolved organic matter as
 653 sensitizer and quencher in the photooxidation of tryptophan. *Environ. Sci. Technol.* 48, 4916-
 654 4924.

655 Janssen, E. M. L., Marron, E., McNeill, K., 2015. Aquatic photochemical kinetics of benzotriazole
 656 and structurally related compounds. *Environ. Sci.: Processes Impacts* 17, 939-946.

657 Lee, E., Glover, C. M., Rosario-Ortiz, F. L., 2013. Photochemical formation of hydroxyl radical
 658 from effluent organic matter: Role of composition. *Environ. Sci. Technol.* 47, 12073-12080.

659 Loiselle, S. A., Azza, N., Cozar, A., Bracchini, L., Tognazzi, A., Dattilo, A., Rossi, C., 2008.
 660 Variability in factors causing light attenuation in Lake Victoria. *Freshwater Biol.* 53, 535-545.

661 Maddigapu, P. R., Bedini, A., Minero, C., Maurino, V., Vione, D., Brigante, M., Mailhot, G.,
 662 Sarakha, M., 2010. The pH-dependent photochemistry of anthraquinone-2-sulfonate.
 663 *Photochemical and Photobiological Sciences* 9, 323-330.

664 Mayo-Bean, K., Moran, K., Meylan, B., Ranslow, P., 2012. Methodology Document for the
 665 ECOlogical Structure-Activity Relationship Model (ECOSAR) Class Program. US-EPA,
 666 Washington DC, 46 pp.

667 Marchetti, G., Minella, M., Maurino, V., Minero, C., Vione, D., 2013. Photochemical
 668 transformation of atrazine and formation of photointermediates under conditions relevant to
 669 sunlit surface waters: Laboratory measures and modelling. *Wat. Res.* 47, 6211-6222.

670 Marchisio, A., Minella, M., Maurino, V., Minero, C., Vione, D., 2015. Photogeneration of reactive
 671 transient species upon irradiation of natural water samples: Formation quantum yields in
 672 different spectral intervals, and implications for the photochemistry of surface waters. *Water*
 673 *Res.* 73, 145-156.

674 Matsushita, T., Kobayasu, N., Hashizuka, M., Sakuma, H., Kondo, T., Matsui, Y., Shirasaki, N.,
 675 2015. Changes in mutagenicity and acute toxicity of solutions of iodinated X-ray contrast
 676 media during chlorination, *Chemosphere* 135, 101-107.

677 McLafferty, F. W., Turecek, F., 1993. Interpretation of mass spectra. Fourth edition, University
 678 Science Books, Mill Valley, California.

679 McNeill, K., Canonica, S., 2016. Triplet state dissolved organic matter in aquatic photochemistry:
 680 reaction mechanisms, substrate scope, and photophysical properties. *Environ. Sci. Processes*
 681 *Impacts* 18, 1381-1399.

682 Page, S. E., Logan, J. R., Cory, R. M., McNeill, K., 2014. Evidence for dissolved organic matter as
 683 the primary source and sink of photochemically produced hydroxyl radical in arctic surface
 684 waters. *Environ. Sci. Processes Impacts* 16, 807-822.

685 Parvez, S., Venkataraman, C., Mukherji, S., 2006. A review on advantages of implementing
 686 luminescence inhibition test (*Vibrio fischeri*) for acute toxicity prediction of chemicals.
 687 *Environ. Int.* 32, 265-268.

688 Plechkova, N. V., Seddon, K. R., 2008. Applications of ionic liquids in the chemical industry
 689 *Chem. Soc. Rev.* 37, 123-150.

690 Puskas, J. E., Chan, S. W. P., McAuley, K. B., Shaikh, S., Kaszas, G., 2005. Kinetics and
 691 mechanisms in carbocationic polymerization: The quest for true rate constants. *J. Polym. Sci.*
 692 *Pol. Chem.* 43, 5394-5413.

693 Richardson, S. D., Ternes, T. A., 2014. Water analysis: emerging contaminants and current issues.
 694 *Anal. Chem.* 86, 2813-2848.

695 Rosario-Ortiz, F. L., Canonica, S., 2016. Probe compounds to assess the photochemical activity of
 696 dissolved organic matter. *Environ. Sci. Technol.* 50, 12532-12547.

697 Silva, M. P., Mostafa, S., McKay, G., Rosario-Ortiz, F. L., Teixeira, A. C. S. C., 2015.
 698 Photochemical fate of amicarbazono in aqueous media: Laboratory measurement and
 699 simulations. *Environ. Eng. Sci.* 32, 730-740.

700 Stepnowski, P., Zaleska, A., 2005. Comparison of different advanced oxidation processes for the
 701 degradation of room temperature ionic liquids *J. Photochem. Photobiol. A.* 170, 45-50.

702 Sun, B., Dong, H. Y., He, D., Rao, D. D., Guan, X. H., 2016. Modeling the kinetics of contaminants
 703 oxidation and the generation of manganese(III) in the permanganate/bisulfite process.
 704 *Environ. Sci. Technol.* 50, 1473-1482.

705 Trivella, A., Stawinoga, M., Dayan, F. E., Cantrell, C. L., Mazellier, P., Richard, C., 2015.
 706 Photolysis of natural beta-triketonic herbicides in water. *Water Res.* 78, 28-36.

707 Vione, D., Minella, M., Maurino, V., Minero, C., 2014. Indirect photochemistry in sunlit surface
708 waters: Photoinduced production of reactive transient species. *Chemistry Eur. J.* 20, 10590-
709 10606.

710 Wenk, J., Eustis, S. N., McNeill, K., Canonica, S., 2013. Quenching of excited triplet states by
711 dissolved natural organic matter. *Environ. Sci. Technol.* 47, 12802-12810.

712 Zeng, T., Arnold, A., 2013. Pesticide photolysis in prairie potholes: Probing photosensitized
713 processes. *Environ. Sci. Technol.* 47, 6735-6745.

714 Zhao, H., Malhotra, S. V., Luo, R. G., 2003. Preparation and characterization of three room-
715 temperature ionic liquids. *Phys. Chem. Liq.* 41, 487-492.